University of Dundee

The structure of lipopolysaccharide transport protein B (LptB) from Burkholderia pseudomallei

Pankov, G.; Dawson, A.; Hunter, W. N.

Communication

The structure of lipopolysaccharide transport protein B (LptB) from *Burkholderia pseudomallei.*

Genady Pankov, Alice Dawson and William N. Hunter

Division of Biological Chemistry & Drug Discovery, School of Life Sciences, University of Dundee, Dundee DD1 5EH, Scotland, UK

Correspondence e-mail: w.n.hunter@dundee.ac.uk

Tel: (0)1382-385745

Fax: (0)1382-385764

PDB reference: 6HS3

Synopsis

The structure of a lipopolysaccharide transport protein B (LptB) is reported. Comparisons with LptB from different bacterial species reveal that the dimeric assembly is independent of interaction with the rest of the transport machinery and significant sequence and structural conservation occurs where LptB interacts with its physiological partners.

Keywords

ABC transporter, ATPase, lipopolysaccharide transport complex, protein-protein interactions

Abstract

The thick outer membrane (OM) of Gram-negative bacteria performs an important protective role against hostile environments, supports cell integrity, contributes to surface adhesion and in some cases also to virulence. A major component of the OM is lipopolysaccharide (LPS), a complex glycolipid attached to a core containing fatty acyl chains. The assembly and transport of lipid A, the membrane anchor for LPS, to the OM begins when a heteromeric $LptB_2FG$ protein complex extracts lipid A from the outer leaflet of the inner membrane. This process requires energy and one component of a heteromeric assembly, LptB, upon hydrolysis of ATP, triggers a conformational change in LptFG in support of lipid A transport. We report a structure of LptB from the intracellular pathogen *Burkholderia pseudomallei.* LptB forms a dimer that displays a relatively fixed structure irrespective of whether in complex with LptFG or in isolation. We discuss highly conserved sequence and structural features that allow LptB to fuel the transport of lipid A.

1. Introduction

Gram-negative bacteria possess a cell wall with double membrane architecture. This protective barrier comprises an inner membrane (IM), the periplasm, which contains a mesh of linked sugars and amino acids, and an outer membrane (OM) with an inner phospholipid layer and outer lipopolysaccharide (LPS) shield (Clifton *et al.,* 2013). LPS consists of lipid A and oligosaccharides (Rietschel *et al*., 1994). Disruption of LPS integrity sensitizes bacteria to antibiotics (e.g. aminoglycosides) as well as to the host immune response and can render the bacteria non-virulent (Delcour, 2009; Tsujimoto, Gotoh & Nishino, 1999; Chapman & Georgopapadakou, 1998). On that basis therefore the proteins that contribute to LPS biosynthesis and OM assembly represent potential targets for antibacterial drug development.

The assembly of components that form the asymmetric IM/OM bilayer requires coordinated synthesis and transport across the periplasm. This process is tightly regulated since the correct assembly of LPS is crucial for the survival of the cell. A lipopolysaccharide transport complex (LPT) of at least seven proteins (Putker, Bos & Tommassen, 2015; Sperandeo *et al*., 2010) is required for export to the OM but the mechanistic details of this process are not completely understood. Transport of LPS begins at the IM where the heterodimeric complex of membrane-bound LptF-LptG proteins act in conjunction with the nucleotide-binding lipopolysaccharide transport protein B (LptB) to form a transmembrane ATP-binding cassette transporter (Narita & Tokuda, 2009; Sherman *et al*., 2014; Sperandeo *et al*., 2010). The transport of LPS requires energy and LptB is thought to bind to the transmembrane LptFG complex, on the cytosolic side, hydrolyse ATP and subsequently trigger a conformational change that supports relocation of LPS through the periplasm.

We are engaged in structural studies to inform on the biosynthesis of different components (Buetow *et al*., 2007; Ulaganathan *et al*., 2007), the organisation and function of the multiprotein complexes involved in LPS assembly and transport. The reagents and models we generate can inform the search for molecules that will compromise OM integrity in bacteria and therefore may have potential in early-stage antibiotic drug discovery (Hunter, 2007). We report a 2.4 Å resolution structure of LptB from the intracellular aerobic pathogen *Burkholderia pseudomallei,* which is the causative agent of melioidosis. This is a particularly difficult to treat infection widespread in tropical regions (Wiersinga *et al*., 2012). Structural features of the cytosolic LptB (*Bp*LptB) will be discussed, and comparisons to close orthologs in

isolation and when bound to LptFG presented.

2. Materials and methods

The gene encoding *B. pseudomallei* LptB, optimized for expression in *Escherichia coli*, (GenScript) was sub-cloned into the expression vector, pET15b-TEV (modified from pET15b, Novagen). The resulting plasmid produces protein with an *N*-terminal hexa-histidine tag that is cleavable by tobacco etch virus (TEV) protease. The plasmid was heat-shock transformed into *E. coli* BL21 (DE3) for production of recombinant protein. Typically, bacteria were cultured at 310 K to an optical density at 600 nm of 0.5-0.6 in Luria-Bertani media containing 50 mg L^{-1} carbenicillin. Gene expression was induced with isopropyl ß-D-1-thiogalactopyranoside (final concentration 1 mM) and growth of the culture continued for approximately 16 h at 296 K prior to harvesting the cells by centrifugation (3500 g for 25 minutes at 277 K). Cells were lysed using a French press at 30 kpsi and the lysate clarified by centrifugation at 37,500 g for 30 min at 277 K. The supernatant was filtered (0.2 μm) and loaded onto a 5 mL HisTrap HP column (GE Healthcare) previously charged with Ni^{2+}, for an initial affinity chromatography step. The target protein was eluted between 460 and 520 mM imidazole, fractions containing *Bp*LptB pooled and treated with TEV protease (1 mg of protease per 10 mg protein) at 296 K for 3 h. Dialysis at room temperature, to remove excess imidazole, was followed by reverse affinity chromatography on the HisTrap column, prior to a final purification step by size exclusion chromatography using a calibrated Superdex [200] 16/60 gel filtration column (GE Healthcare) in 50 mM HEPES-NaOH pH 7.5, 250 mM NaCl, 5 mM $MgCl_2$, 10% glycerol and 500 μM ATP. Initial attempts at purification gave rise to heavy precipitation and loss of material during dialysis. The addition of ATP to the buffer alleviated these solubility issues. The theoretical mass of *Bp*LptB is approximately 28 kDa and in size exclusion chromatography a well-defined profile suggested the presence of a single species of approximate molecular mass 42 kDa. Fractions containing LptB were pooled and exchanged into 50 mM Tris-HCl, 150 mM NaCl pH 7.5, 5 mM $MgCl_2$ and 500 μM ATP and concentrated using centrifugal force (Sartorius) prior to crystallisation trials. Sample purity was assessed by sodium dodecyl sulphate polyacrylamide gel electrophoresis. The approximate yield of *Bp*LptB was 1.6 mg L^{-1} of *E. coli.*

2.2. Crystallisation

A search for crystallisation conditions was initiated using commercially available screens and identified a starting point that was optimized. *Bp*LptB gave crystals in sitting-drop vapour-diffusion experiments when 2 μL of a protein solution at 4 mg mL^{-1} in 50 mM Tris-HCl pH 7.5, 150 mM NaCl, 0.5 mM ATP, 5 mM MgCl$_2$ was mixed with an equal volume of reservoir (0.2 M MgCl$_2$, 0.1M Tris-HCl pH 8.5 and 30% w/v PEG4000). Needle-shaped crystals, typically with dimensions of 15 x 15 x 800 μm, appeared over 5 days at 296 K.

2.3. X-ray data collection and processing, structure determination and refinement

Crystals were cryo-protected in mother liquor supplemented with 10 % (v/v) ethylene glycol, then flash cooled in liquid nitrogen prior to shipment to the Diamond Light Source synchrotron facility (Harwell Science and Innovation Campus, Oxfordshire). Diffraction data were subsequently collected using a micro-focused beamline I24, λ = 0.9686 Å, and Pilatus3 6M detector.

Data to 2.4 Å were integrated using MOSFLM (Battye *et al*., 2011) then processed with AIMLESS (Evans, 2011). Pronounced radiation damage was noted and influenced which data were included in the refinement. A single polypeptide from *Paraburkholderia phymatum* LptB (PDB code 4WBS) with 90% sequence identity provided a model for molecular replacement calculations in PhaserMR (McCoy *et al*., 2007). Two such polypeptides were positioned in the unit cell and the resulting electron density map allowed the *Bp*LptB sequence to be incorporated using *COOT* (Emsley *et al.*, 2010) with refinement in *REFMAC5* (Murshudov *et al.*, 2011). Weak non-crystallographic symmetry restraints were employed during refinement.

Several rounds of electron and difference density map inspection, model manipulation and refinement led to the incorporation of solvent, chloride ions and a number of rotamers for selected side chains. *MOLPROBITY* (Chen *et al.*, 2010) was used at different stages to monitor model geometry in combination with the validation tools provided in *COOT*. Crystallographic statistics are presented in Table 1.

3. Results and discussion

The structure of *Bp*LptB was determined by molecular replacement and refined to 2.4 Å resolution. The asymmetric unit contains two polypeptide chains, which are labelled A and B. There was no reliable electron density for the first 12 residues in chain A, the

first seven and last residue in chain B and they are absent from the model. Each *Bp*LptB polypeptide presents a characteristic fold resembling ATPases of other ABC transporter systems (Figure 1A). The asymmetric unit, a dimer, is depicted in Figure 1B. The amino acid sequence of *Bp*LptB is presented in Figure 2, aligned with sequences of four orthologues, marked up to identify characteristic features of this protein family. These sequences, for which structures are available, were retrieved from the Uniprot database ({ HYPERLINK "https://www.uniprot.org/" }) and aligned using *T-COFFEE* multiple sequence alignment (Noterdame *et al.,* 2000). Conserved motifs were highlighted using *Jalview* (Waterhouse *et al.,* 2009).

The characteristic features of LptB are the Walker A and B motifs, and four loops involved in creating the ATPase catalytic site (Sherman *et al*., 2014; Figure 2). These six segments are highly conserved across species (Figure 2). The ATP:Mg^{2+} binding site is formed by Walker A (G-x(4)-GK-[TS]) and Walker B (hhhhDE) motifs (Walker *et al*., 1982; Hanson & Whiteheart, 2005). The Q-loop is a conformationally variable region located between Walker A and Walker B motifs with a conserved glutamine (Gln97) participating in nucleotide binding. This residue is proposed to help couple ATP hydrolysis to conformational changes in the TM domains of LptFG (Sherman *et al*., 2014). In addition, a characteristic signature motif or C-loop, is placed near the Walker B motif and also interacts with ATP. In LptB the D-loop with a conserved Asp186, interacts with the Walker A motif of the partner subunit (Davidson *et al.,* 2008). The H-loop, carrying a residue of functional importance, His212 is a part of a conformational switch region, which participates in coordination of the γ-phosphate of ATP (Sherman *et al*., 2014).

Although present in the crystallisation conditions there was no evidence in the electron density for either ATP or Mg^{2+}. The absence of cofactor in the structure may be explained by the ionic strength of the crystallisation conditions and the fact that the ATP-binding site is a relatively open cleft located on the surface of the protein. Two chloride ions were found associated with the ATP-binding domain with one interacting with His212. The presence of chloride, a component of the crystallisation condition, is consistent with a biologically relevant site, where a negatively charged entity can bind.

The LptB polypeptides, which display similar conformations, form a dimer of approximate dimensions 85 x 50 x 25 Å. The elongated structure of the *Bp*LptB dimer may contribute to the observed gel-filtration data where the elution volume corresponded to a MW ≈ 42 kDa, intermediate between the predicted molecular weight

of monomer (MW ≈ 28 kDa) and dimer (MW ≈ 56 kDa). A structural overlay of 240 Cα atoms common to the two polypeptides in the *Bp*LptB asymmetric unit results in a (root-mean-square deviation) r.m.s.d. of 0.88Å. This value falls in the range of r.m.s.d.s noted for superposition of the two LptB polypeptides in the asymmetric unit of structures for four orthologues, 0.50 to 1.11 Å, for which sequences are shown in Figure 2. The LptB subunit fold is conserved and displays no major conformational differences irrespective of whether the cofactor is present in the structure or not. Cα superposition of individual *Bp*LptB monomers on the subunits A and B of homologous structures results in an average r.m.s.d. of 1.84 Å for 16 such overlays. Structural comparisons of the dimeric LptB assembly indicates that these subunits interact in a similar fashion either in isolation or when part of the LptB$_2$FG complex. A structural overlay of the *Bp*LptB dimer with LptB polypeptides in LptB$_2$FG complexes from *Pseudomonas aeruginosa* (Figure 3; PDB: 5X5Y; Quingshang *et al*., 2017) and *Klebsiella pneumoniae* (PDB: 5L75; Dong *et al*., 2017) provided an r.m.s.d from the *Bp*LptB dimer of 1.86 Å and 2.24 Å respectively indicating that the dimeric structures are similar. These values are derived from the least-squared overly of 460 and 441 Cα positions respectively.

Areas where two LptB subunits interact with each other involve the Walker A motif and D-loop and these part of the structure share a high degree of sequence conservation in LptB orthologs (Figure 2). Analysis of *Bp*LptB using *Pisa* (Krissinel & Henrick, 2007) indicates that each subunit contributes approximately 6.6 % of the surface (around 800 Å^2) to dimer formation with an estimated solvation free energy gain of - 6.2 Δ^{i}G kcal/mol. For the LptB dimers forming part of LptB$_2$FG complexes in *P. aeruginosa* and *K. pneumonia* these values are around 700 Å^2; -3.4 Δ^{i}G kcal/mol and 600 Å^2; -6.3 Δ^{i}G kcal/mol respectively. These values are low compared to the commonly accepted threshold where >900 Å^2 lost solvent accessible surface area and with Δ^{i}G <-8 kcal/mol is considered to be an indication of a dimer (Jones & Thornton, 1996). Nevertheless, the size-exclusion chromatography profile of *Bp*LptB and the consistent arrangement of subunits in crystal structures of orthologs suggest that *Bp*LptB does indeed display the structure of a functional dimer.

The structural conservation with orthologs suggests that LptB does not undergo any major structural changes when it forms a complex with the LptFG heterodimer. An overlay of the LptB components of the LptB$_2$FG complexes from *P. aeruginosa* (PDB:

5X5Y) and the structure reported here provides a model to identify which parts of *Bp*LptB might be involved in complex formation with the membrane bound heterodimer. The LptFG assemblies interact with LptB through placement of an α-helix, called the "coupling helix" (Dong *et al*., 2017), into grooves on the LptB dimer that are formed by a continuous stretch of residues from Pro83 through to Arg103 in *Bp*LptB. This segment of the polypeptide comprises the Q-loop and a region preceding it, both of which are highly conserved in LptB sequences (Figure 2). There is also a contribution from the C-loop. Seven residues, placed in or at the side of the LptB grooves and C-loop have been identified as important to formation of a functional LptB$_2$FG complex (Dong *et al.,* 2016; Sherman *et al.,* 2014, Simpson *et al*., 2016). The overlay positions the seven residues in *Bp*LptB at the interface with LptF and LptG. In *Bp*LptB these residues correspond to His85, Ser89, Tyr94, Phe102, Arg103, Val114, and Arg161. These residues are highlighted in Figure 2. Five of the residues are strictly conserved in the five sequences shown, Val114 is conserved in four of them with an isoleucine observed in one. Ser89 is substituted with arginine in three of the sequences. This strictly conserved phenylalanine, Phe102, is essential for interaction with the cognate-binding partners (Sherman *et al.*, 2014; Simpson *et al*., 2016). It is of note also that the antibiotic novobiocin binds *E. coli* LptB to activate the LPS transporter system, by directly interacting at the Phe102-Arg103 site (May *et al.*, 2017).

Pairwise alignments of five sequences that create LptFG heteromers were carried out. The sequences were derived from the species listed in Figure 2. The sequence identity for LptF pairs ranged from 27 to 85%, for LptG from 26 to 93%. A key aspect of LptFG interactions with LptB involves a serine glutamate dipeptide unit, in a helical conformation on the N-terminal segment of the former (Dong *et al*., 2017). This dipeptide is strictly conserved in all LptF and LptG sequences. Our observations support the conclusion that the protein-protein interactions that create a stable LptB$_2$FG complex are maintained across species (Dong *et al*., 2017). The targeted disruption of this protein-protein interface might then interfere with lipid A transport from the IM to the OM and in so doing compromise the viability of a wide range of gram-negative pathogens.

4. Concluding remarks

A robust and reproducible protocol for recombinant protein production of *Bp*LptB in *E. coli* has been established, protein purified, crystallisation conditions established and the crystal structure determined at 2.4 Å resolution. Comparison of *Bp*LptB to its orthologs, characterised individually or in the form of LptB$_2$FG complexes indicates that the molecular features responsible for the LptB-LptB interactions and associations with LptFG appear widely conserved. Disruption of the relevant protein-protein assemblies by targeting the relevant interfacial regions offers opportunities to develop novel antibiotics.

Table 1. Crystallographic statistics for *Bp*LptB.

Resolution range (Å)	63.7 - 2.4
Space Group	$P\,2_1\,2_1\,2_1$
Unit cell parameters	*a*=52.79 *b*= 74.23,
	c= 124.38 Å
Wavelength (Å)	0.9686
No. Reflections [a]	71991 (7291)
No. Unique Reflections	19107 (1977)
R_{merge} [b]	0.119 (0.703)
R_{pim} [c]	0.082 (0.496)
Completeness (%)	97.0 (98.0)
$\langle I/\sigma(I)\rangle$	10.2 (5.8)
Multiplicity	3.8 (3.7)
$CC_{1/2}$	0.982 (0.487)
Mosaicity (°)	0.32
Wilson *B*-factor (Å^2)	22.5
R_{work} [d] (%)	0.205
R_{free} [e] (%)	0.270
R.m.s.d bonds (Å)	0.0085
R.m.s.d angles (°)	1.2528
Total protein residues	493
Total protein atoms	3777
Average protein *B*-factor (Å^2)	29.16
DPI (Å) [f]	0.6355
Ramachandran plot:	
Favored (%)	97
Allowed (%)	3
Outliers (%)	0
Additional groups:	
Solvent (No./Average *B* (Å^2))	113 / 26.83
Chloride (No./Average *B* (Å^2))	2 / 30.54

[a] Values in parentheses refer to the highest resolution shell. [b] $R_{merge} = \sum h \sum i ||(h,i) - \langle I(h)\rangle \sum h \sum i\, I(h,i)$; where I(*h,i*) is the intensity of the *i*th measurement of reflection *h* and <I(*h*)> is the mean value of I(*h,i*) for all *i* measurements. [c] R_{pim} is the same as R_{merge} but independent of redundancy. [d] $R_{work} = \sum hkl ||F_o|-|F_c||/\sum/F_o/$, where F_o is the observed structure factor amplitude and the F_c is the structure-factor amplitude calculated from the model. [e] R_{free} is the same as R_{work} except calculated with a subset, 5%, of data that are excluded from refinement calculations. [f] The Diffraction-component Precision Index as defined by Cruickshank, 1999.

References

Battye, T. G., Kontogiannis, L., Johnson, O., Powell, H. R. & Leslie, A. G. (2011). *Acta Crystallogr. D. Biol. Crystallogr.* **67**, 271–281.

Buetow, L., Smith, T. K., Dawson, A., Fyffe, S. & Hunter, W. N. (2007). *Proc. Natl. Acad. Sci. U S A.* **104**, 4321-4326.

Chapman, J. S., Georgopapadakou, N. H. (1998). *Antimicrob Agents Chemother.* **32,** 438–442.

Chen, V. B., Arendall, W. B., Headd, J. J., Keedy, D. A., Immormino, R. M., Kapral, G. J., Murray, L. W., Richardson, J. S. & Richardson, D. C. (2010). *Acta Crystallogr. D. Biol. Crystallogr.* **66,** 12–21.

Clifton, L. A., Skoda, M. W. A., Daulton, E. L., Hughes, A. V., Le Brun, A. P., Lakey, J. H. & Holt, S. A. (2013). *J. Royal. Soc. Interface*, **10**. DOI:10.1098/rsif.2013.0810

Cruickshank, D. W. (1999). *Acta Crystallogr. D. Biol. Crystallogr.* **55**, 583-601.

Davidson, L. A., Dassa, E., Orelle, C. & Chen, J. (2008). *Microbiol. Mol. Biol. Rev.* **72**, 317–364.

Dong H., Zhang Z., Tang, X., Paterson, N. G. & Dong, C. (2017). *Nature Communications* **8**, 222.

Emsley, P., Lohkamp, B., Scott, W. G. & Cowtan, K. (2010). *Acta Crystallogr. D. Biol. Crystallogr.* **66,** 486–501.

Evans, P. R. (2011). *Acta Crystallogr. D. Biol. Crystallogr.* **67**, 282–292.

Evans, P. R. & Murshudov, G. N. (2013). *Acta Crystallogr. D. Biol. Crystallogr.* **69**, 1204–1214.

Hanson, P. I. & Whiteheart, S. W. (2005). *Nat. Rev. Mol. Cell Biol.* **6**, 519–529.

Hunter, W. N. (2007). *Biochem Soc. Trans.* **35**, 980-984.

Jones, S. & Thornton, J. M. (1996). *Proc. Natl. Acad. Sci. U S A.* **93**, 13-20.

Krissinel, E. & Henrick, K. (2007). *J. Mol. Biol.* **372**, 774-797.

May, J. M., Owens, T. W, Mandler, M. D., Simpson, B. W., Lazarus, M. B., Sherman, D. J., Davis, R. M., Okuda, S., Massefski, W., Ruiz, N. & Kahne, D. (2017). *J Am Chem Soc.* **139**, 17221-17224.

McCoy, A. J., Grosse-Kunstleve, R. W., Adams, P. D., Winn, M. D., Storoni, L. C. & Read, R. J. (2007). *Appl. Crystallogr.* **40**, 658-674.

Murshudov, G. N., Skubák, P., Lebedev, A. A., Pannu, N. S., Steiner, R. A., Nicholls, R. A., Winn, M. D., Long, F. & Vagin, A. A. (2011). *Acta Crystallogr. D. Biol. Crystallogr.* **67**, 355–367.

Narita, S. & Tokuda, H. (2009). *FEBS Letts.* **583**, 2160–2164.

Notredame, C., Higgins, D. G. & Heringa, J. (2000). *J. Mol. Biol.* **302**, 205-217.

Okuda, S., Sherman, D. J., Silhavy, T. J., Ruiz, N. & Kahne, D. (2006). *Nat. Rev. Microbiol.* **14**, 337-345.

Putker, F., Bos, M. P. & Tommassen, J. (2015). *FEMS Microbiology Reviews*, **39**, 985–1002.

Qingshan, L., Xu, Y., Shan, Y., Huigang, S., Kun, W., Le, X., Guangyu, Z., Chuanqi, S., Tingting, L., Dianfan, L., Xinzheng, Z., Min, Z. & Yihua, H. (2017). *Nature Structural & Molecular Biology,* **24**, 469–474.

Relcour, A. H. (2009). *Biochim Biophys Acta* **1794**, 808-816.

Rietschel, E. T., Kirikae, T., Schade, F. U., Mamat, U., Schmidt, G., Loppnow, H., Ulmer, A. J., Zähringer, U., Seydel, U., Padova, F., *et al.* (1994). *FASEB J,* **8**, 217-225.

Sherman, D. J., Lazarus, M. B., Murphy, L., Liu, C., Walker, S., Ruiz, N. & Kahne, D. (2014). *Proc. Nat. Acad. Sci. USA*, **111**, 4982-4987.

Sherman, D. J., Xie, R., Taylor, R. J., George, A. H., Okuda, S., Foster, P. J., Needleman, D. J. & Kahne, D. (2008). *Science* **111,** 798-801.

Simpson, B. W., Owens, T. W., Orabella, M. J., Davis, R. M., May, J. M., Trauger, S. A., Kahne, D. & Ruiz, N. (2016) *MBio.* **7**. e01729-16.

Sperandeo, P., Villa, R., Martorana, A.M., Samalikova, M., Grandori, R., Dehò, G. & Polissi, A. (2010). *Journal of Bacteriology*, **193**, 1042–1053.

Tsujimoto, H., Gotoh, N. & Nishino, T. (1999). *J. Infect. and Chemo.* **5**, 196–200.

Ulaganathan, V., Buetow, L. & Hunter, W. N. (2007) *J. Mol. Biol.* **369**, 305-312.

Waterhouse, A. M., Procter, J. B., Martin, D. M. A., Clamp, M. & Barton, G. J. (2009). *Bioinformatics* **25,** 1189-1191

Walker, J. E., Saraste, M., Runswick, M. J. & Gay, N.J. (1982). *EMBO J.* **8,** 945–951.

Wiersinga, W.J., Currie, B. J. & Peacock, S. J. (2012). *N. Engl. J. Med.* **367**, 1035-1044.

Figure 1. A. A Cα trace of *Bp*LptB subunit A. The characteristic motifs of this protein family are colored blue and labelled. B. A van der Waals surface representation of the *Bp*LptB dimer. Subunit A is colored light grey, subunit B yellow. The groves between Pro83 and Arg103 where proposed interactions with *Bp*LptFG take place are shown in dark grey. The position of two residues that are highly conserved across LptB sequences, Phe102 and Arg103 shown.
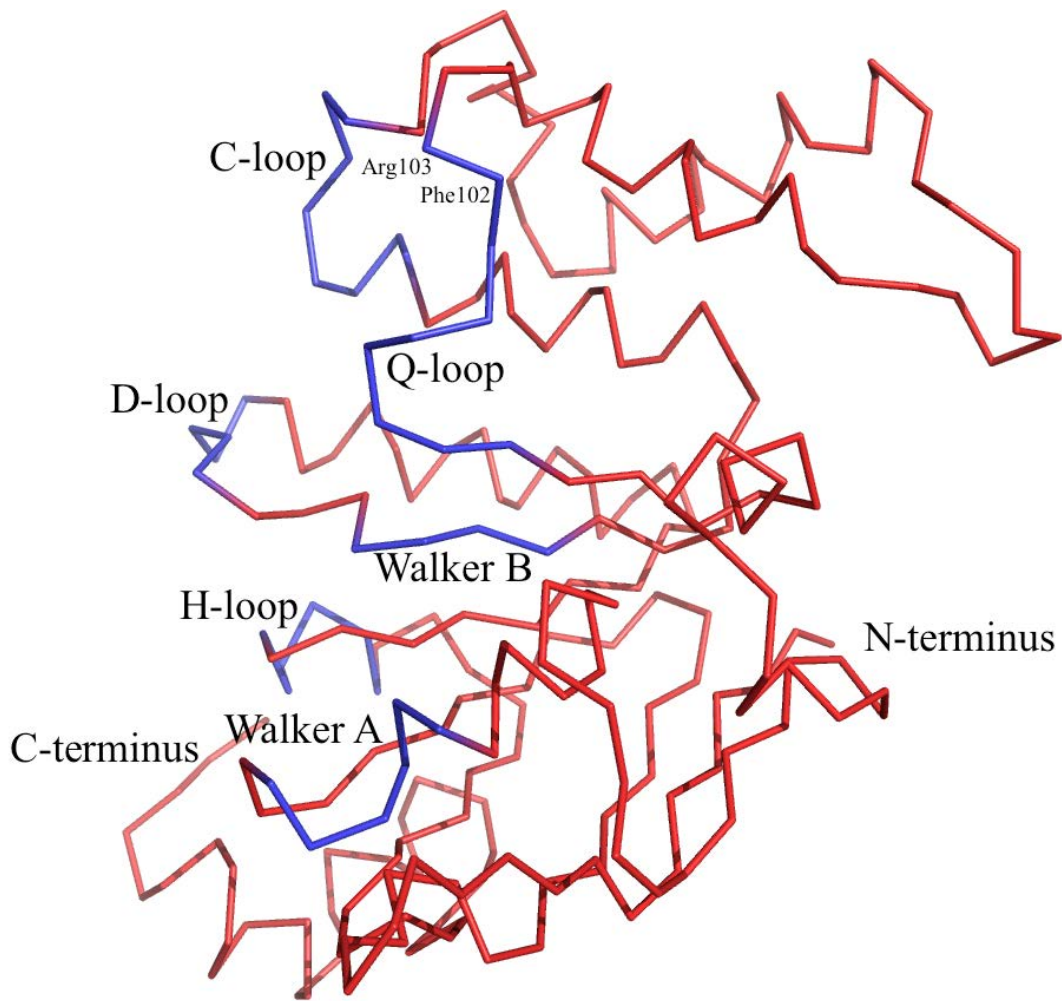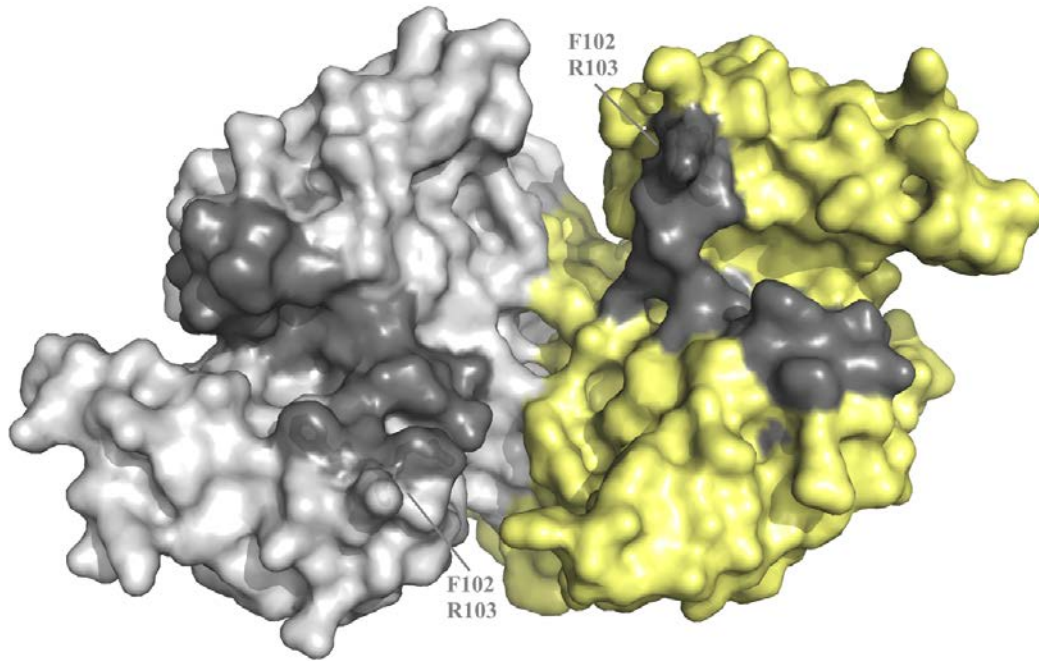

Figure 1A

Figure 1B.

Figure 2. Sequence comparison of five LptB orthologs for which structures are known. *B. pseudomallei* (this work), *B. phymatum* (PDB: 4WBS; 90% sequence identity), *E. coli* (PDB: 4P31; 59% sequence identity), *K. pneumonia* (PDB: 5L75; 58% sequence identity), and *P. aeruginosa* (PDB: 5X5Y; 56% sequence identity). Sequences are aligned and coloured by conservation using an 80% identity threshold. Conserved and functionally important regions are labelled and the seven residues implicated in complex formation with LptFG are marked with a red star.

Figure 3. A Cα overlay of the *Bp*LptB dimer with LptB polypeptides in LptB$_2$FG complexes from *P. aeruginosa*. *Bp*LptB subunits A and B are coloured in black and blue respectively. *P. aeruginosa* LptB is shown in red.
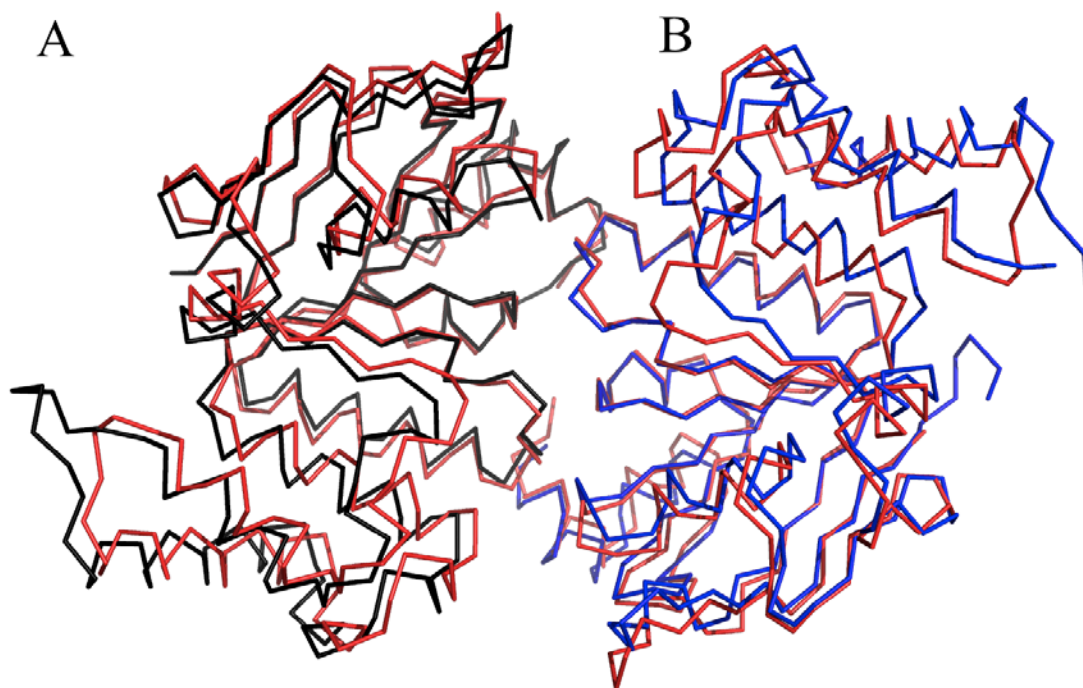

Figure 3.